Thermodynamics of Stacking Faults in GaAs-based System revealed by in-situ heating in TEM

Wenyu Hu[a,#], Manyu Dang[b,#], Jiawei Dong[c,#], Yong Deng[d], Huiwen Deng[b], Mingchu Tang[b], Gan Wang[a,*], Xiaoyi Wang[c,*], Yang Qiu[e,*], Huiyun Liu[b] and Thomas Walther[f].

[a] Department of Physics, Southern University of Science and Technology, Shenzhen 518055, China.

[b] Department of Electronic and Electrical Engineering, University College London, Torrington Place, London, WC1E 7JE, UK.

[c] Southwest Minzu University, State Ethnic Affairs Commission, Chengdu 610041, China.

[d] Department of Materials, Sun Yat-Sen University, Guangzhou 510000, China.

[e] Core Research Facilities, Southern University of Science and Technology, Shenzhen 518055, China.

[f] School of Electrical & Electronic Engineering, University of Sheffield, Sheffield S1 3JD, United Kingdom.

# These authors have equal contribution to this work.

* Corresponding author: wangg@sustech.edu.cn; 80300024@swun.edu.cn; qiuy@sustech.edu.cn

ABSTRACT: Stacking faults (SFs) are a type of two-dimensional defect that can significantly degrade the performance of III-V semiconductor devices. In this study, we investigate the thermal evolution of intrinsic SFs in (In)GaAs-on-Si systems using in-situ heating in an aberration-corrected scanning transmission electron microscopy. Our results indicate that chiral intrinsic SFs near the InGaAs/GaAs interface undergo thermally induced migration and interaction, leading to the formation of Lomer-Cottrell locks at 700 °C. Between 200 and 700 °C, SFs exhibit sliding behaviour, which triggers their reaction into a characteristic three-layer defect (TLD) structure, which could be quickly annihilated during the baking environment. Using Lorentz transmission electron microscopy (LTEM) to image magnetization configurations, we observed the formation of intrinsic stacking fault (SF)-induced magnetic vortices. These vortices arise from the competition between the Heisenberg exchange interaction and the Dzyaloshinskii-Moriya interaction (DMI). Notably, as field-driven dipole oscillations intensify, the magneto-Stark effect enables manipulation of transitions between out-of-plane and in-plane magnetic vector fields. This work advances the understanding of defect dynamics in III-V compound semiconductors and provides new strategies for tailoring crystal quality during epitaxial growth.

KEYWORDS: III-V group semiconductor, InGaAs/GaAs interface, stacking faults, transmission electron microscope, in-situ heating

1. INTRODUCTION

To achieve monolithic photonic integration on Si, the epitaxial growth of GaAs-based semiconductors on silicon represents a promising approach for fabricating high-performance laser diodes[1-4]. However, the significant lattice mismatch between Si and GaAs induces substantial local strain near the Si/GaAs interface, which can trigger the generation of lattice defects[Error! Reference source not found.-7], including Lomer dislocations[8], 60° dislocations (type II dislocation)[9] and stacking faults[10]. As a typical two-dimensional defect, a stacking fault (SF) is bounded by a pair of Shockley partial dislocations[Error! Reference source not found.]. The breaking of local atomic periodicity could lead to the formation of electronic trapping states within the bandgap, leading to the degradation of device performance [12,13].

As a fundamental technique for reducing dislocation density, thermal annealing is commonly employed to enhance the crystal quality of as-grown GaAs epilayer films. According to the mechanism proposed by Jung et al.[14], dislocation sliding induced by thermal cyclic annealing facilitates the annihilation of threading dislocations. Similarly, in experiments conducted by Guo et al.[15], the elimination of dislocations occurs by lateral migration of randomly distributed inversion domains. Although the thermal response of dislocations has been extensively investigated at the atomic scale[16,17], research on thermally induced SF dynamics still remains scarce—particularly regarding SF reactions under applied external thermal load. While often considered detrimental to optoelectronic device performance, the behaviour of stacking faults is a critical factor in the mechanical properties of semiconductors. For instance, in materials like silicon carbide (SiC), the movement and interaction of stacking faults are known to enhance the material's resistance to radiation damage by providing pathways for the recombination of point defects[18-21]. This highlights that a fundamental understanding of SF thermodynamics is not only crucial for minimizing their negative impact but also for harnessing their properties in functional materials. However, the thermal dynamics of SFs in III-V systems like GaAs, which underpin modern photonics, remain comparatively less explored, particularly their atomic-scale evolution and interaction under thermal stress. Yet, the influence of temperature has not been incorporated into the existing physical model proposed[22], and its role remains poorly understood.

Furthermore, since there has been no in-situ research on magnetic properties of SFs in GaAs, the magnetic evolution during thermally induced SF reactions has not been described so far either.

In this work, the thermal evolution of intrinsic SFs in (In)GaAs system has been directly observed via in-situ heating in an aberration-corrected scanning transmission electron microscopy (AC-STEM). In contrast to Lomer-Cottrell locks formed by chiral intrinsic SF pairs, this study investigates the transformation of intrinsic SFs into three-monolayer SFs at the atomic scale. These three-layer defects (TLDs) are highly sensitive to external thermal load and can be quickly annihilated by heating. Of note, by applying a "hysteresis loop"-like external magnetic excitation to suppress the magneto-Stark effect at 0 mT, the parity symmetry breaking of stacking faults in GaAs can lead to a non-zero Dzyaloshinskii-Moriya (DM) coefficient. This arises from unpaired electron spins localized at SF sites, which are responsible for forming out-of-plane magnetic vortices. Subsequently, as the external magnetic field strength varies, the magneto-Stark effect emerges, enabling the transition between out-of-plane and in-plane magnetization textures.. Therefore, it can be concluded that the competition between Heisenberg exchange and DMI is a dominant factor in triggering the formation of magnetic vortices at local intrinsic SFs. However, when the magneto-Stark effect is induced by external magnetic excitation, it enables the alignment of the magnetization vector field along the (1-10) atomic plane. During the annihilation of TLDs in a thermal environment, the weakening of carrier localization is expected to reduce the number of unpaired electron spins and suppress the magneto-Stark effect at local stacking faults (SFs), ultimately leading to demagnetization of these regions.

2. EXPERIMENTAL SECTION

2.1 EPITAXY PROCESS

The InGaAs/GaAs dislocation filter layer (DFL) sample was grown in a Veeco Gen 930 solid-source molecular beam epitaxy system, and on n-type Si (001) substrate with a 4° offcut towards [110]. Silicon substrates were degassed at 600 ℃ for one hour, and the substrate was monitored by an in-situ RHEED during a 950 ℃ surface deoxidation process. A 5 nm AlAs nucleation layer was grown via migration-enhanced epitaxy at 375 ℃, followed by the epitaxy of a 1.35 μm GaAs buffer layer. Then, the temperature range for thermal cycle annealing (TCA) was set from 320 ℃ to 680 ℃, with a holding time of 7 mins at temperatures of 320 ℃, while maintaining arsenic overpressure and performing 8 cycles to protect the surface. After the TCA process, the

InGaAs DFL was grown at 470 ℃, consisting of 150 nm $In_{0.05}Ga_{0.95}As$, 200 nm $In_{0.1}Ga_{0.9}As$, and 300 nm $In_{0.05}Ga_{0.95}As$, respectively. More details of epitaxy can be found in our previous work[23].

2.2 IN-SITU SAMPLE PREPARATION AND CHARACTERIZATION

The preparation of TEM specimens for in-situ observation was carried out in a Thermo Fisher Helios 600i scanning electron microscope equipped with a gallium focused ion beam (FIB). A 100 nm chromium (Cr) protection layer was deposited on the surface by thermal evaporation in a high vacuum resistance evaporation coating equipment (VZZ-300, Beijing Micro Nano Vacuum Technology Co., LTD). This was followed by the ion beam assisted deposition of a 2 μm thick platinum (Pt) layer. A 10×5×2 μm^3 lamella was extracted by using a 30 kV focused Ga ion beam with the beam current of 9.3-2.5 nA, afterwards, the lamella was transferred to a Fusion heating E-chip (E-FHDN-VO, Protochips Inc.). The specimen was further thinned to about 100 nm by a 30 kV Ga ion beam with a beam current down to 0.43 nA and finally 23 pA. To minimize the surface oxidation and Ga implantation, the final surface polishing was carried out in a Fischione Nanomill 1040, where the accelerating voltage and beam current of argon ion beam were set to 500 V and 130 pA, respectively.

Atomic resolution images were acquired on a Thermo Fisher Titan Themis G2 double aberration corrected transmission electron microscope at 300 kV, the probe current was set to about 70 pA for increasing the signal to noise ratio. The E-chip TEM specimen was fixed in a Protochips Fusion AX in-situ heating and biasing holder (Protochips Inc.), where the temperature can be varied within a range of 25 ℃-1200 ℃. During the in-situ heating process, the heating/cooling rate was set at 10 ℃/min, consistent with the TCA process. The magnetic response of SFs was studied in a Thermo Fisher Talos F200X equipped with a Lorentz lens, where the external magnetic flux density can be continuously varied from –2 T to +2 T. The Fresnel-contrast (defocused) imaging mode was adopted to image the magnetic streaks from local SFs.

3. Results and discussion

To investigate the structural evolution of SFs under thermal load, the existence of SFs must first be confirmed first by atomic imaging. At room temperature, pairs of chiral intrinsic SFs (Figure 1b and c) were observed near the $In_{0.05}Ga_{0.95}As$ /GaAs interface (marked by blue square in Figure 1a). An intrinsic SF forms when two bounded Shockley partial dislocations (90° and 30°) allow the dissociation of a 60° perfect dislocation along $(0\bar{1}\bar{1})$ or $(10\bar{1})$ crystal plane[24]. The corresponding Burgers

vectors responsible for intrinsic SF formation can be expressed as[22]:

$$a/2\ [0\bar{1}\bar{1}] = a/6\ [\bar{1}\bar{2}\bar{1}] + a/6\ [1\bar{1}\bar{2}] \quad (1)$$

or

$$a/2\ \ [10\bar{1}]\ \ = a/6\ [21\bar{1}] + a/6\ [1\bar{1}\bar{2}] \quad (2)$$

where a is the lattice constant. To confirm that the intrinsic SF in Figure 1 b) undergoes dissociation of a 60° perfect dislocation, the atomic image shown in Figure 1d was simulated by Dr Probe software[25]. In Figure 1c, when probing the structure along [110] zone axis, a 54.7° angle is observed between the misaligned atomic column and the $(1\bar{1}\bar{2})$ atomic plane, which correlates well with our observation in Figure 1b.

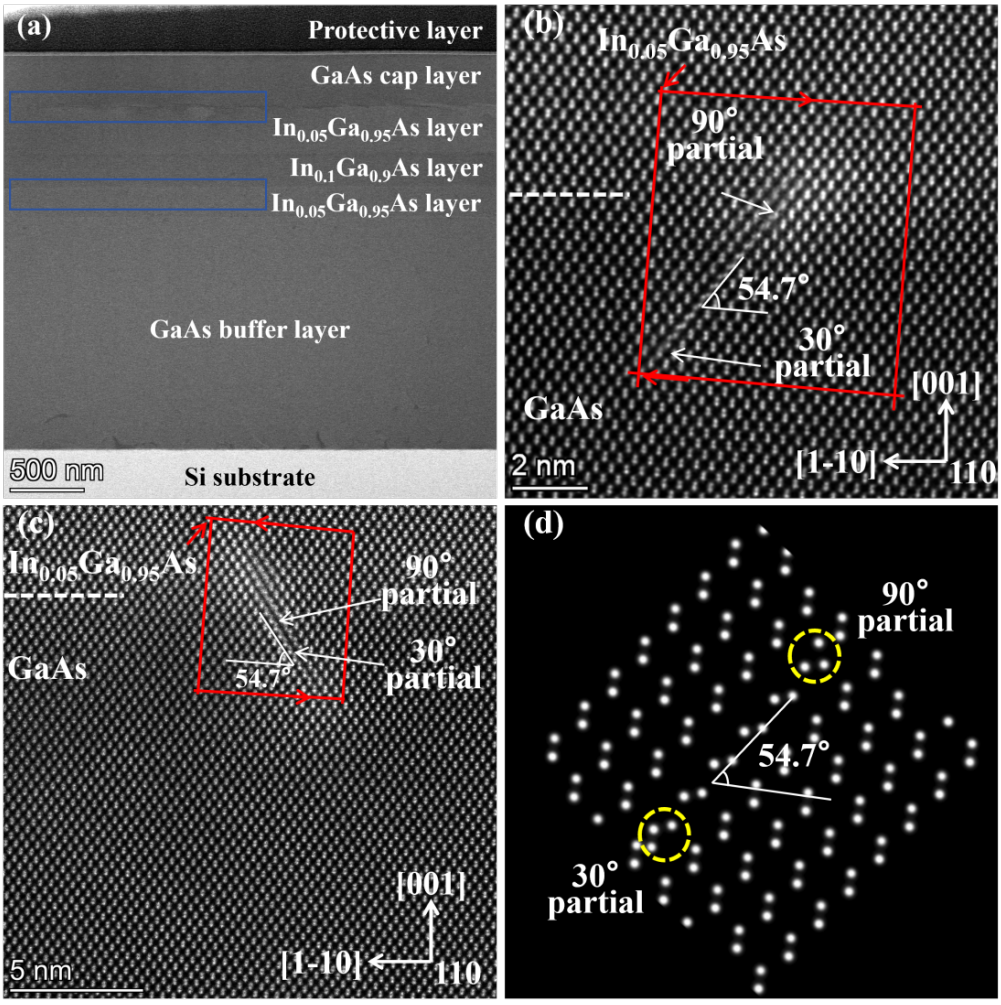

Figure 1. Cross-sectional view of sample. (a) STEM-DF image of basic structure, (b,c) STEM-HAADF images of the $In_{0.05}Ga_{0.95}As$/GaAs interface. (d) simulated STEM-HAADF image calculated for the SF atomic structure in figure 1(b).

For the intrinsic SF in Figure 1c, which exhibits a chiral atomic orientation opposite to the SF in Figure 1b, the possible Burger vector equation can be written as follows:

$$a/2\,[0\bar{1}1] = a/6\,[\bar{1}\bar{2}1] + a/6\,[1\bar{1}2] \quad (3)$$

or

$$a/2\,[101] = a/6\,[211] + a/6\,[1\bar{1}2] \quad (4)$$

Since two chiral SFs have Burger vectors with mirror symmetry, a 54.7° angle between the chiral intrinsic SF and the [110] projection plane is also observed in Figure 1c.

According to the theorem proposed by Gangopadhyay et al.[22], external thermal loading provides the kinetic energy required for intrinsic SFs to slip along the <111> directions. This facilitates the merging and interaction of intrinsic SF pairs with opposite chirality, ultimately forming a Lomer-Cottrell lock (stair-rod dislocation). The reaction of chiral intrinsic SFs to generate Lomer-Cottrell lock is described as a linear superposition of their Burgers vectors. The resulting Lomer-Cottrell lock has a Burgers vector of $a/6\,[1\bar{1}0]$, which does not facilitate SF slipping due to the orthogonality between $\{1\bar{1}0\}$ and {111} plane. This geometric constraint pins the Lomer-Cottrell lock during thermal annealing[26]. To supply sufficient kinetic energy for SF slipping, the TEM specimen was heated to 700°C and held at this temperature for 10 minutes, which was followed by natural cooling to room temperature (Figure 2a and 2b). In Figure 2a, several triangular defects in the GaAs buffer layer were formed after thermal annealing. Atomic-resolution imaging (Figure 2b) reveals that these defects arise from the merging of two intrinsic SFs via their 30° partial dislocations. Since the 30° partials are separated by Ga-As pairs, the isolated atomic columns should consist only of Ga atoms in [110] projection[22]. To verify this, atomic-scale elemental mapping of Ga and As was performed via energy-dispersive X-ray spectroscopy (Figure 2c), and the isolated atomic columns marked by purple circles were confirmed to be Ga atoms. These results confirm that pairs of intrinsic SFs with opposite chirality form stable Lomer-Cottrell locks at 700 °C. Notably, while Abrahams et al.[27],[28] predicted that homochiral intrinsic SF pairs should react to form extrinsic SFs, no such evidence was observed in Figure 2a.

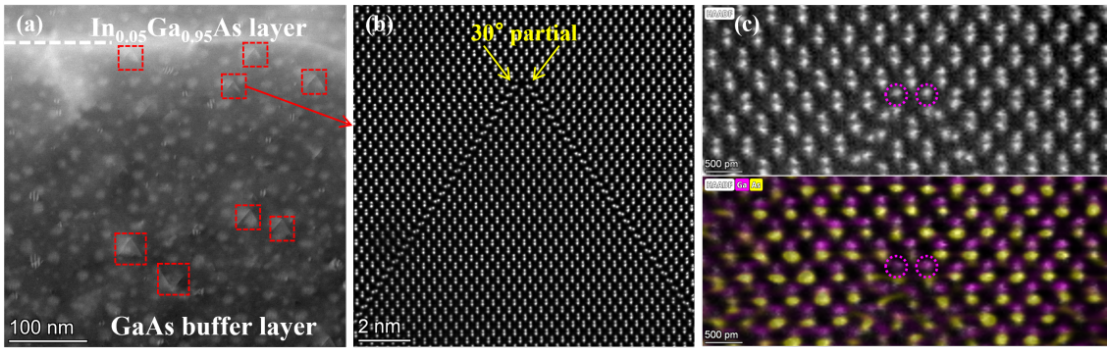

Figure 2. Sample was heated to 700 °C then cooled back to RT (a) basic structure, (b) high resolution

STEM-HAADF image of the triangular defect, (c) atomic-resolution EDS map (HAADF-Ga-As colormix) of the 30° partials area in figure 2(b).

To investigate the physical mechanism underlying the absence of extrinsic SFs, the TEM specimen of the as-grown DFL sample was heated to 300°C—a temperature expected to overcome the kinetic energy threshold for intrinsic SF gliding. Afterwards, heating was immediately ceased, and the sample was naturally cooled to room temperature, where the mobility and reaction of SFs could only be driven by residual thermal energy. The corresponding atomic images are shown in Figure 3. As depicted in Figure 3c and 3d, the target intrinsic SF at the InGaAs/GaAs interface has completely vanished during the specimen cooling stage, indicating that the residual thermal energy is sufficient to drive the gliding of intrinsic SFs. Interestingly, several short defects are observed in the squares marked in Figure 3e, and the distinctive three-layer structure of these defects (Figure 3f) cannot be attributed to any previously reported SF type.

Inspired by Abrahams et al.[27], the conventional three-layer-fault plane can be formed by a single pair of intrinsic and extrinsic SFs. The schematic diagram (Figure 3g) shows the formation mechanism of a three-layer SF. During the annealing processing, the vacancies condense at the initial SF end to form three overlapping intrinsic faults, these will be bounded by Frank partials, each having Burgers vector equal to $a/3[\bar{1}1\bar{1}]$. During the evolution of the three-layer SF driven by the external heating field, thermal stress induces the rapid expansion of some dislocation rings and Shockley partial dislocations, promoting the fracture zone to restore its complete crystal sequence. The extended Frank partial dislocation reacts with the Shockley partial dislocation to form a complete dislocation:

$$a/6\ [\bar{2}1\bar{1}] + a/6\ [01\bar{1}] = a/3\ [\bar{1}1\bar{1}] \quad (5)$$

Complete dislocation slip occurs and moves away from the defect area, leaving behind a residual layered fault, which is defined by a portion of dislocation with Burgers vectors of $a/6[\bar{4}1\bar{1}]$[27]. When the remaining dislocations reach the surface of the sample, the dissociation of the Burgers vector may result in a slip-off complete dislocation ($a/2[\bar{1}10]$) and a Shockley partial dislocation with Burgers vector of $a/2[\bar{1}\bar{2}\bar{1}]$ (moving in the opposite direction to the other end of the layer dislocation):

$$a/6\ [\bar{4}1\bar{1}] - a/2\ [\bar{1}10] = a/6\ [\bar{1}\bar{2}\bar{1}] \quad (6)$$

When the Shockley partial dislocation meets its counterpart (from the other side of the fault), they will annihilate one another[27]. In this way, the entire faulted defect is annihilated. The end result is a defect-free region, which completes the SF annihilation

process. However, one would expect to observe a superimposed atomic image of faulted and during the final stage of three-layer SF annihilation. To verify this, the atomic model of the three-layer SF and the corresponding simulated HAADF image along the [110] projection direction are presented at the bottom of Figure 3g. By wrapping the (110) facet of the three-layer SF model with a bilayer of unfaulted GaAs (Figure 3g), the simulated image at the bottom of Figure 3g matches perfectly with the unrecognized defect (Figure 3f), indicating the nearly complete annihilation of the three-layer SF. Therefore, it can be confirmed that the absence of extrinsic SF at 700 °C is associated with the reaction of homochirality SFs, which leads to the formation of three-layer SFs. The expansion of the unfaulted Shockley partial via thermally induced gliding restores a perfect planar sequence in the slipped region, resulting in the rapid annihilation of three-layer SFs at high temperature.

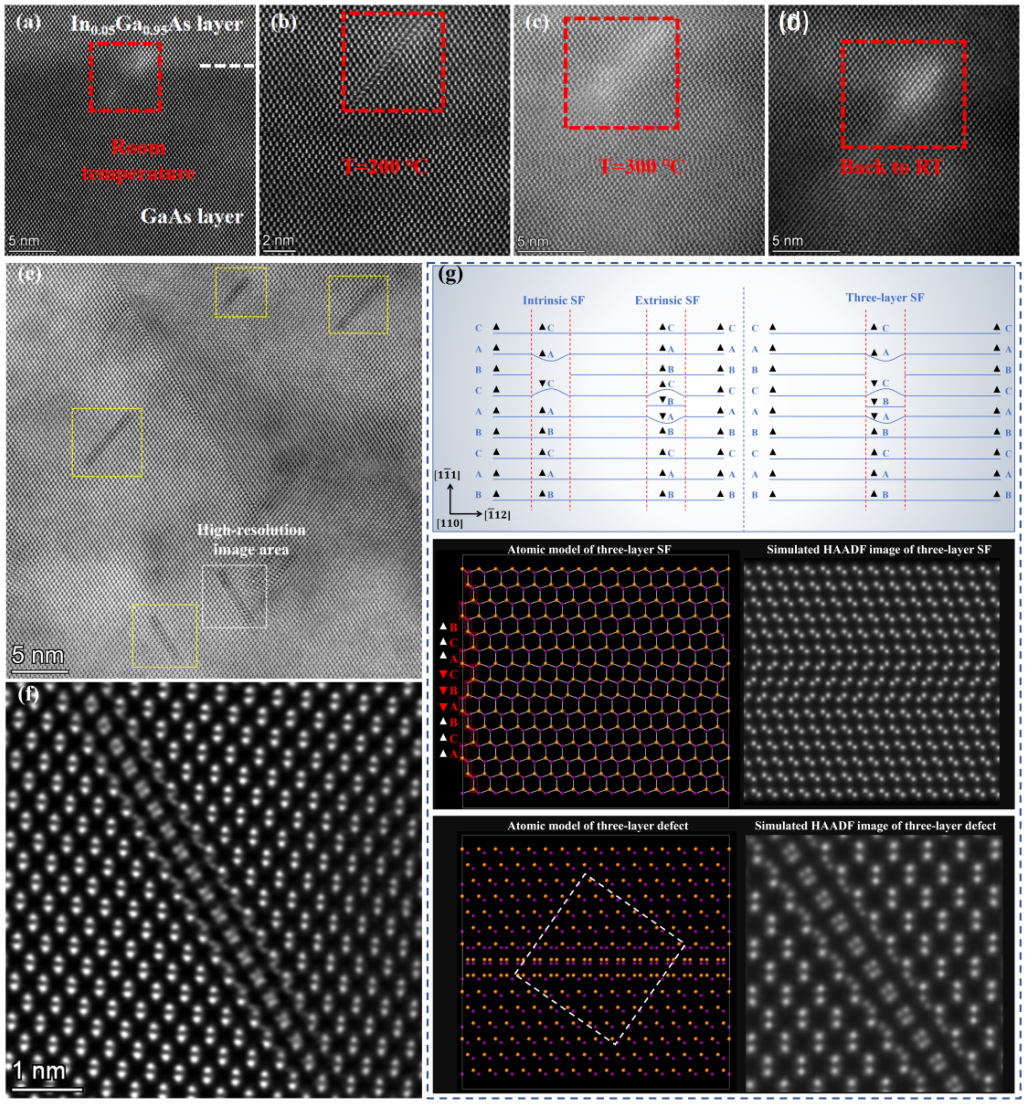

Figure 3. Cross-sectional STEM-HAADF images of sample at different temperatures (a) Room temperature of intrinsic SF, (b) 200 °C, (c) 300 °C, (d) back to room temperature. Cross-sectional

view of GaAs buffer layer after heating to 300 ºC and cooling back to room temperature (e) STEM-BF image, (f) high-resolution image of the area within the white square, (g) model of the planar scheme (top), atomic model and related simulated HAADF image of three-layer SF (middle) and TLD (bottom).

In existing theories, the magnetic response of a single stacking fault is governed solely by the magneto-Stark effect[29], where local dipole oscillation driven by external magnetic excitation is responsible for shifting the emission wavelength. However, this conclusion may be overly simplistic. As a typical parity-symmetry-breaking crystal, GaAs can exhibit a non-zero DMI coefficient (see Equation S2 in the supplementary information). Once unpaired electron spins are generated—such as those localized at stacking faults—the competition between the Heisenberg spin exchange and DMI can promote the formation of magnetic vortices [29]. Since the magnetization vortex of SFs has never been revealed in the GaAs system, the magnetic property of SFs in GaAs remains elusive. Therefore, to investigate the magnetic texture at sub-micron scale, measurements of the magnetic structure of SFs were carried out using a Lorentz TEM at room temperature, with the application of "hysteresis loop"-like external magnetic excitation. The magnetic field strength was fixed within the range of –200 mT and 200 mT at a step size of 50 mT (Figure 4). As shown in Figure 4, vortex structures were observed in the vicinity of the InGaAs/GaAs interface, where the maximum density of SFs is located (Figure 1a). By varying the external magnetic field strength, a field-driven magnetic response was confirmed exclusively at these micron-scale structures (Figure 4a-4c), whereas no visible contrast perturbation was observed in the TLD regions (Figure 4d-4f). In addition, since the observed SFs are approaching complete annihilation, the weakening of exciton localization is expected to demagnetize the SF regions. Therefore, it was proven that the field-driven magnetic response can only be triggered in the existing SFs.

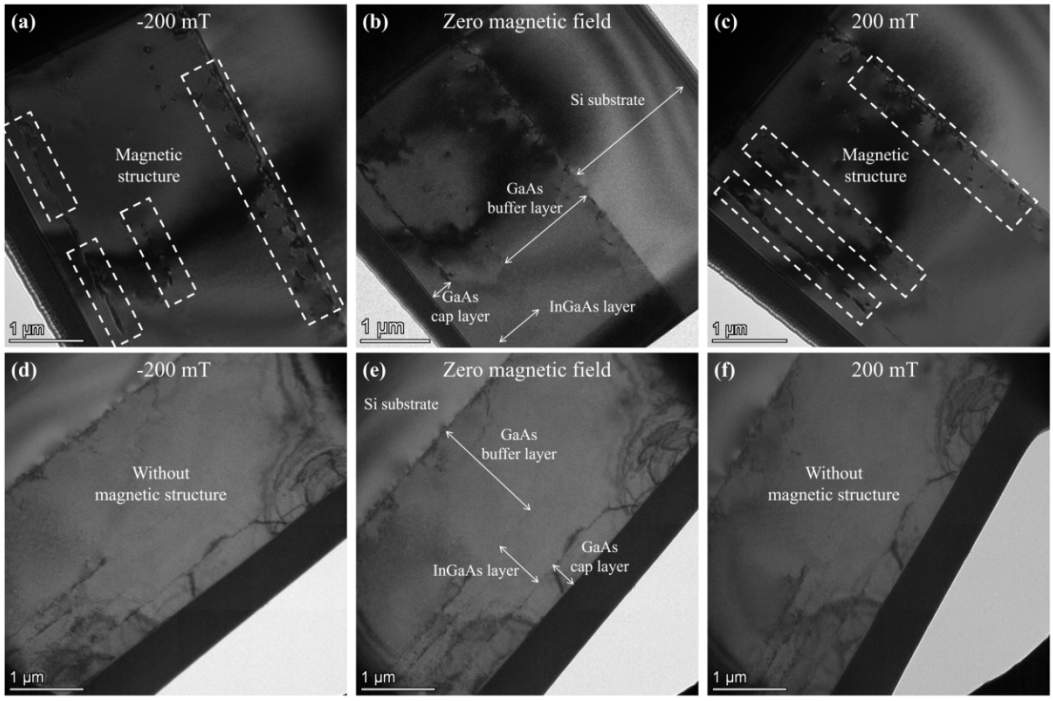

Figure 4. Lorentz TEM with Fresnel imaging mode of the sample at room temperature (a) with –200 mT applied magnetic field, (b) zero magnetic field, (c) with 200 mT applied magnetic field; Lorentz TEM with Fresnel imaging mode of the sample heated to 300 ºC and cooled back to room temperature (d) with –200 mT applied magnetic field, (e) zero magnetic field, (f) with 200 mT applied magnetic field.

To investigate the magnetization configuration in detail, the in-plane magnetic textures of corresponding magnetic structures in the SF-containing region were mapped using the transport of intensity equation (TIE) (Figure 5). As shown in Figure 5b-5j, all the magnetic structures exhibit a clear vortex-like magnetization configuration. Particularly under zero external magnetic field (0 mT, Figure 5b) where the magneto-Stark effect is minimized, the formation of magnetic vortices can be attributed to the competition between Heisenberg exchange and DMI in this parity-symmetry-breaking system (intrinsic stacking faults in GaAs). The localized electrons at these faults with unpaired spins are responsible for forming local magnetic vortices (see supplementary material for detailed mathematical expressions). Of note, a distinct out-of-plane magnetic vortex is observed in Figure 5e-5h. However, by reversing the external magnetic excitation, the magnetization vectors gradually aligned within the (1-10) foil plane, which represents an out-of-plane to in-plane magnetic moment transition. Since the magneto-Stark effect can modulate the spin texture along the [111] direction, its enhancement enables the realignment of magnetic moments within the (1-10) foil plane.

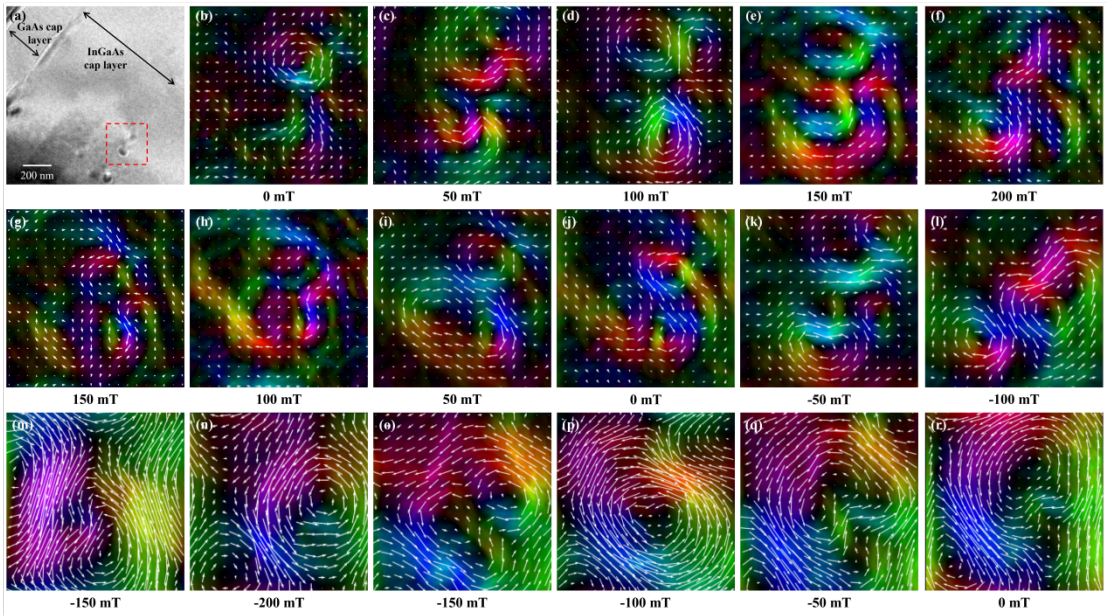

Figure 5. Magnetic field dependence of SF structure in real-space Lorentz TEM images at room temperature and the corresponding spin texture obtained by TIE analysis (a) TEM image of magnetic bubbles with 200 mT magnetic field, (b) 0 mT, (c) 50 mT, (d) 100 mT, (e) 150 mT, (f) 200 mT, (g) 150 mT, (h) 100 mT, (i) 50 mT, (j) 0 mT, (k) -50 mT, (l) -100 mT, (m) -150 mT, (n) -200 mT, (o) -150 mT, (p) -100 mT, (q) -50 mT (r) 0 mT.

4. Conclusions

In summary, the mechanism underlying chirality dependent SFs reactions was revealed. Above the threshold temperature of SFs propagation (200℃), a pair of SFs with same chirality is expected to form Lomer-Cottrell locks. This type of defect is proven to be thermally stabilized, capable of maintaining its atomic structure up to 700℃. In contrast, instead of forming extrinsic SFs during thermal preservation (300℃), SFs of opposite chirality are expected to generate TLDs, such defects are highly sensitive to external thermal loads, enabling the TLD to be rapidly annihilated in a thermal environment. Consequently, near the final stage of TLD annihilation, one would expect to observe an “unrecognized” defect structure, which corresponds to the superimposed atomic image of faulted and unfaulted atomic layers. Through LTEM analysis, the local field-driven magnetic response indicates that the generation of magnetization configuration of intrinsic SFs is attributed to the competition between Heisenberg spin exchange and Dzyaloshinskii-Moriya interaction, while the magneto-Stark effect can only manipulate the transition between out-of-plane and in-plane magnetic vortices. For TLD approaching complete annihilation, carrier localization in the fault plane is significantly weakened, resulting in apparent demagnetization of

stacking faults (SFs). This occurs due to the absence of unpaired electron spins at local SF sites, combined with the weakening of the magneto-Stark effect. Our findings advance the understanding of SF reaction dynamics and local magnetic properties, providing valuable guidance for the development of high-performance GaAs-based electronic and photonic devices.

Acknowledgments

This work was supported by the UK Engineering and Physical Sciences Research Council (EP/Z532848/1, EP/X015300/1, EP/T028475/1, EP/S024441/1, and EP/P006973/1).

AUTHOR DECLARATIONS

Conflict of Interest

The authors declare that they have no known competing financial interests or personal relationships that could have appeared to influence the work reported in this paper.

Author Contributions

Wenyu Hu: Data curation (equal); Formal analysis (equal); Investigation (equal); Validation (equal); Visualization (lead); Writing-original draft (lead); Software (lead). **Manyu Dang**: Data curation (equal); Validation (equal); Investigation (equal). **Jiawei Dong**: Data curation (equal); Validation (equal); Visualization (supporting). **Yong Deng**: Data curation (supporting); Visualization (supporting). **Huiwen Deng**: Visualization (supporting). **Mingchu Tang**: Methodology (equal); Writing-review & editing (equal). **Gan Wang**: Writing-review & editing (equal); Resources (equal); Funding acquisition (equal); **Xiaoyi Wang**: Methodology (equal); Writing-review & editing (equal); Investigation (equal); Validation (supporting); Project administration (equal). **Yang Qiu**: Methodology (equal); Writing-review & editing (equal); Project administration (equal); Resources (equal). **Huiyun Liu**: Methodology (equal); Writing-review & editing (equal); Project administration (equal). **Thomas Walther**: Methodology (supporting); Writing-review & editing (supporting).

References

[1] A. H. Atabaki, S. Moazeni, F. Pavanello, H. Gevorgyan, J. Notaros, L. Alloatti, M. T. Wade, C. Sun, S. A. Kruger, H. Meng, K. A. Qubaisi, I. Wang, B. Zhang, A. Khilo, C. V. Baiocco, M. A. Popović, V. M. Stojanović and R. J. Ram, Integrating photonics with silicon nanoelectronics for the next generation of systems on a chip. *Nature*. **556**, 349-354 (2018).

[2] S. Mauthe, Y. Baumgartner, M. Sousa, Q. Ding, M. D. Rossell, A. Schenk, L. Czornomaz and K. E. Moselund, High-speed III-V nanowire photodetector monolithically integrated on Si. *Nat. Commun.* **11**, 4565 (2020).

[3] E. Tournié, L. M. Bartolome, M. R. Calvo, Z. Loghmari, D. A. Díaz-Thomas, R. Teissier, A. N. Baranov, L. Cerutti and J.-Baptiste Rodriguez, Mid-infrared III-V semiconductor lasers epitaxially grown on Si substrates. *Light. Sci. Appl.* **11**, 165 (2022).

[4] P. Wen, P. Tiwari, S. Mauthe, H. Schmid, M. Sousa, M. Scherrer, M. Baumann, B. I. Bitachon, J. Leuthold, B. Gotsmann and K. E. Moselund, Waveguide coupled III-V photodiodes monolithically integrated on Si. *Nat. Commun*. **13**, 909 (2022).

[5] Y. Du, B. Xu, G. Wang, Y. Miao, B. Li, Z. Kong, Y. Dong, W. Wang and H. H. Radamson, Review of Highly Mismatched III-V Heteroepitaxy Growth on (001) Silicon. *Nanomaterials.* **12**, 741 (2022).

[6] E. T. Hughes, M. Dumont, Y. Hu, D. Liang, R. G. Beausoleil, J. E. Bowers and K. Mukherjee, Dislocation Formation and Filtering in III-V Regrowth on GaAs Bonded on Si. *Cryst. Growth Des.* **22**, 5852 (2022).

[7] S. Liu, B. Ratiu, H. Jia, Z. Yan, K. M. Wong, M. Martin, M. Tang, T. Baron, H. Liu, Q. Li, Effective InAsP dislocation filtering layers for InP heteroepitaxy on CMOS-standard (001) silicon. *Appl. Phys. Lett.* **125**, 082102 (2024).

[8] S. Flores, D. F. Reyes, T. Ben, V. Braza, N. J. Bailey, M. R. Carr, R. D. Richards and D. Gonzalez, Exploring the formation of InAs(Bi)/GaAs QDs at two growth-temperature regimes under different Bi supply conditions. *Appl. Surf. Sci.* **607**, 154966 (2023).

[9] A. Vilà, A. Cornet, J. R. Morante, P. Ruterana, M. Loubradou and R. Bonnet, Structure of 60° dislocations at the GaAs/Si interface. *J. Appl. Phys.* **79**, 676-681 (1996).

[10] D. Gerthsen, C. B. Carter, Stacking-Fault Energies of GaAs. *Phys. Status. Solidi. A*. **136**, 29-43 (1993).

[11] Y. A. R. Dasilva, R. Kozak, R. Erni and M. D. Rossell, Structural defects in cubic semiconductors characterized by aberration-corrected scanning transmission electron microscopy. *Ultramicroscopy*. **176**, 11-22 (2017).

[12] T. Mano, A. Ohtake, T. Kawazu, H. T. Miyazaki and Y. Sakuma, Low Dark Current Operation in InAs/GaAs(111)A Infrared Photodetectors: Role of Misfit Dislocations at the Interface. *ACS Appl. Mater. Interfaces* **15**, 29636-29642 (2023).

[13] S. A. Church, S. Hammersley, P. W. Mitchell, M. J. Kappers; L. Y. Lee, F. Massabuau, S. L. Sahonta, M. Frentrup; L. J. Shaw; D. J. Wallis; C. J. Humphreys, R. A. Oliver, D. J. Binks and P. Dawson, Effect of stacking faults on the photoluminescence spectrum of zincblende GaN. *J. Appl. Phys.* **123**, 185705 (2018).

[14] D. Jung, P. G. Callahan, B. Shin, K. Mukherjee, A. C. Gossard, J. E. Bowers, Low threading dislocation density GaAs growth on on-axis GaP/Si (001). *J. Appl. Phys.* **122**, 225703 (2017).

[15] W. Guo, L. Chen, H. Xu, Q. Chen, K. Liu, T. Luo, J. Jiang, H. Wu, G. Chen, H. Lu and J. Ye, Annihilation of Nanoscale Inversion Domains in Nitrogen-Polar AlN under High-Temperature Annealing. *Cryst. Growth Des.* **23**, 229–235 (2023).

[16] E. T. Hughes, M. Dumont, Y. Hu, D. Liang, R. G. Beausoleil, J. E. Bowers and K. Mukherjee, Dislocation Formation and Filtering in III-V Regrowth on GaAs Bonded on Si. *Cryst. Growth Des.* **22**, 5852 (2022).

[17] C. Gong, A. W. Robertson, K. He, G. D. Lee, E. Yoon, C. S. Allen, A. I. Kirkland and J. H. Warner, Thermally Induced Dynamics of Dislocations in Graphene at Atomic Resolution. *ACS Nano* 9, 10, 10066-10075 (2015).

[18] J. Yamasaki, S. Inamoto, Y. Nomura, H. Tamaki and N. Tanaka, Atomic structure analysis of stacking faults and misfit dislocations at 3C-SiC/Si(001) interfaces by aberration-corrected transmission electron microscopy. *J. Phys. D: Appl. Phys.* **45**, 494002 (2012).

[19] A. Sarikov, A. Marzegalli, L. Barbisan, M. Zimbone, C. Bongiorno, M. Mauceri, D. Crippa, F. La Via and L. Miglio, Mechanism of stacking fault annihilation in 3C-SiC epitaxially grown on Si(001) by molecular dynamics simulations. *Cryst. Eng. Comm.* **23**, 1566-1571(2021).

[20] H. Sen, N. Daghbouj, B. Li, A. AlMotasem, F. Ge, L. Zhang, M. Callisti and T. Polcar, Interaction of Stacking Faults with point/extended defects in Fe-He irradiated 6H-SiC. *Acta. Mater.* **256**, 119129 (2023).

[21] Z. Wang, L. Zhang, A. AlMotasem, B. Li, T. Polcar and N. Daghbouj, Exploring defect behavior in helium-irradiated single-crystal and nanocrystalline 3C-SiC at 800°C: A synergy of experimental and simulation techniques. *Acta. Mater.* **279**, 120281 (2024).

[22] A. Gangopadhyay, A. Maros, N. Faleev and D. J. Smith, Strain relaxation in low-

mismatched GaAs/$GaAs_{1-x}Sb_x$/GaAs heterostructures. *Acta. Mater.* **162**, 103-115 (2019).

[23] M. Dang, H. Deng, S. Huo, R. R. Juluri, A. M. Sanchez, A. J Seeds, H. Liu and M. Tang, The growth of low-threadingdislocation-density GaAs buffer layers on Si substrates. *J. Phys. D: Appl. Phys.* **56**, 405108 (2023).

[24] A. Gangopadhyay, A. Maros, N. Faleev and D. J. Smith, Atomic structure of dissociated 60° dislocations in GaAs/$GaAs_{0.92}Sb_{0.08}$/GaAs heterostructures. *Scr. Mater.* **153**, 77-80 (2018).

[25] J. Barthel, Dr. Probe: A software for high-resolution STEM image simulation. *Ultramicroscopy*, **193**, 1-11 (2018).

[26] C. R. Weinberger and W. Cai, The stability of Lomer – Cottrell jogs in nanopillars. *Scr. Mater.* **64**, 529-532 (2011).

[27] M. S. Abrahams and C. J. Buiocchi, Mechanism of Thermal Annihilation of Stacking Faults in GaAs. *J. Appl. Phys.* **41**, 2358-2365 (1970).

[28] H. Holloway, Diffraction by Faulted Close-Packed Lattices: An Analytic Solution for Systems Without Long-Range Correlation of Stacking Symbols. *J. Appl. Phys.* 40, 4313-4321 (1969).

[29] M. V. Durnev, M. M. Glazov, X. Linpeng, M. L. K. Viitaniemi, B. Matthews, S. R. Spurgeon, P. V. Sushko, A. D. Wieck, A. Ludwig and K. M. C. Fu, Microscopic model for the stacking-fault potential and the exciton wave function in GaAs. *Phys. Rev. B* **101**, 125420 (2020).

[30] J. P. Liu, Z. Zhang, and G. Zhao, Skyrmions: topological structures, properties, and applications. *CRC Press*, 2016.

[31] G. M. Wysin, F. G. Mertens, A. R. Völkel and A.R. Bishop, Mass and Momentum for Vortices in Two-Dimensional Easy-Plane Magnets. *Springer, Boston*, 1994, 177-186.